

# Influence of Turbine and Compressor Wheel Mass and Inertia on the Rotor Dynamics of Turbocharger

J. Knotek<sup>a</sup>, P. Novotný<sup>a</sup>, O. Maršálek<sup>a</sup>, P. Raffai<sup>a</sup>, J. Dluhoš<sup>a</sup>

<sup>a</sup>*Institute of Automotive Engineering, Brno University of Technology, Czech Republic.*

## Keywords:

*Turbocharger  
Rotor dynamics  
Floating ring bearing  
Compressor mass  
Turbine mass*

## ABSTRACT

*This paper describes the influence of the compressor and turbine wheel mass and inertia change on the turbocharger rotor dynamics. The model of the turbocharger is presented, the hydrodynamic model of the journal bearing is described and assembly of the whole model in MBS is also presented. The article presents various results describing rotor dynamics on which the influence of compressor and turbine wheel mass and inertia change is discussed.*

## Corresponding author:

*Ing. Jiří Knotek  
Institute of Automotive Engineering,  
Brno University of Technology,  
Czech Republic.  
E-mail: knotek@iae.fme.vutbr.cz*

© 2016 Published by Faculty of Engineering

## 1. INTRODUCTION

The modern trend in automotive industry is to minimize emissions of vehicle power unit. One of the ways which many car and engine manufacturers are using is to introduce turbocharger into the power unit. The turbocharger not only helps to reduce emissions but also increases output power. The rising number of turbocharged engines produced constrains the turbocharger manufacturers to increase effectiveness, reliability and usability while preserving or reducing the costs. Moreover, all of this has to be achieved within a short development time.

To achieve effective and suitable design for specific turbocharger in short development time,

the turbocharger manufacturers are using a set of turbochargers. Turbochargers in these sets usually share the shaft, bearing and central housing, etc., and the compressor and turbine wheel differ. However, to adjust the turbocharger design for specific engine, the turbocharger manufacturers usually have to modify the compressor and/or turbine wheel design.

With the change of the compressor and turbine wheel geometry the mass, inertia and usually even the location of the center of gravity change. This leads to the need for numerous measurements and this significantly increases the costs of the development. To have in possession some kind of simulation tool which would enable to simulate the influence of the

turbocharger rotor design change on rotor dynamics would significantly decrease the number of measurements needed, and consequently, the costs of the development.

## 2. STATE OF THE ART

Rotor based machinery usually operates at constant speed or in quite narrow range of operating speeds but a turbocharger operates in wide speed range. Modern turbocharger operates up to 300 000 min<sup>-1</sup>. This fact makes turbocharger modelling quite a challenging area. First attempts to model turbocharger rotor behaviour were through the usage of the simplest rotor models but this solution is not sufficient for the wide speed range. The major breakthrough method was introduced by Schweizer in [1-2]. He used MBS based turbocharger rotor model enriched by journal bearing model for turbocharger rotor dynamics prediction. Since then, most of the models have been using this concept worldwide – MBS based rotor model with specialized journal bearing model. This trend can be demonstrated on the work of Tian, who used this type of model to study influence of the rotor unbalance and engine vibration on turbocharger rotor dynamics and published the results in [3-4].

## 3. TURBOCHARGER MODEL

The turbocharger model presented in this paper is based on the MBS system, namely the MSC Adams. This corresponds to the state of the art presented above. And advantage of this procedure lies in the usage of commercial software for rotor modelling. The rotor model is then enriched by journal bearing model. Both journal bearing model and rotor model are briefly introduced below.

### 3.3 Hydrodynamic journal bearing model background

Turbocharger bearing has to provide sufficient damping and exhibit little oil film based instabilities. This has to be achieved while preserving low friction losses. This leads to usage of, essentially, two types of journal bearing in the turbocharger design – i.e. the fully-floating ring bearing and semi-floating ring

bearing. Standard arrangement of this type of bearing is shown in Fig. 1. The floating ring in the semi-floating ring bearing has a restricted rotation around rotor axis of rotation, on the other hand, the floating ring in the fully floating ring bearing is able to rotate freely. The rational decision then is to model the fully-floating ring bearing first, because the semi-floating ring bearing can be then created by disabling the rotation of the floating ring.

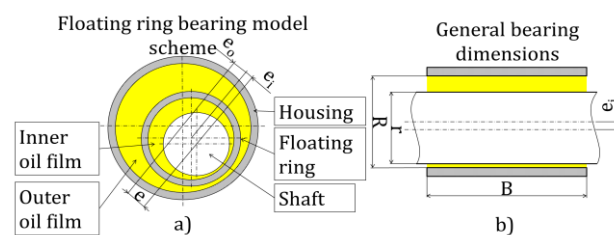


**Fig. 1.** General arrangement of the journal bearing model used: a) Floating ring bearing model scheme, b) Standard bearing dimensions.

Each oil film of the fully-floating ring bearing is considered to be a plain journal bearing. This leads to employment of the Reynolds equation. This equation is based on the Navier-Stokes equation and continuity equation transformed for cylindrical shapes of the bearing oil gap. The full form of the equation has been simplified and modified into the following form [5]:

$$\frac{\partial}{\partial x} \left( h^3 \frac{\partial p}{\partial x} \right) + \frac{\partial}{\partial y} \left( h^3 \frac{\partial p}{\partial y} \right) = 6\eta \left( U \frac{dh}{dx} + 2 \frac{dh}{dt} \right) \quad (1)$$

where:  $h$  is oil film thickness,  $\eta$  is dynamic oil viscosity and  $U$  is effective speed.

The previous equation is solved by iterative numerical method, namely Gauss-Seidel method. To speed up the solution, the finite difference method is incorporated using variable integration steps and multi-grid strategy. The result of this equation is pressure distribution over the bearing width and diameter.

The main parameter that influences distribution of the hydrodynamics pressure is the height of the oil film  $h$ . Its non-dimensional form is calculated by equation [6]:

$$H = 1 + (\varepsilon - Z \cdot \gamma \cdot (1 - \varepsilon)) \cdot \cos \varphi + \delta \cdot Z \cdot \sin \varphi \cdot \sqrt{1 - (\varepsilon + (1 - \varepsilon) \cdot |\gamma|^2)}, \quad (2)$$

where:  $\varepsilon$  is journal eccentricity,  $\varphi$  is dimension along bearing circumference,  $Z$  is a dimension

along bearing width and  $\gamma$  and  $\delta$  are journal tilt angles.

As shown in the equations above, the pressure distribution largely depends on the oil film height. The solution considers not only journal eccentricity, but also the tilt of the journal. The journal tilt is described by two angles –  $\delta$ ,  $\gamma$ .  $\gamma$  is the tilt angle in the plane of the smallest oil gap and  $\delta$  is the angle in the plane perpendicular to it.

The result of the Reynolds equation solution is the hydrodynamic pressure over the bearing width and diameter. The pressure distribution can be divided into two parts – negative and positive pressure. However, the nature of oil film form is able to transfer only positive pressure and not the negative one (tension). This phenomenon is usually called the cavitation condition.

The consideration of the cavitation and pin tilting angles provides more detailed turbocharger rotor dynamics analysis and consequently leads to better understanding of the relation between oil film instability and shapes of individual eigen-modes.

To increase the speed of the rotor dynamics solution, the solution of hydrodynamic pressure is performed in advance. The hydrodynamic pressure distribution is solved based on the width to diameter ratio and the result is in the form of dimensionless forces and torques. The forces and torques are recorded in the resultant tables (hydrodynamic databases). These hydrodynamic databases are then transferred to the MBS and thus the journal bearing model can be introduced into the MBS. The dimensionless forces and torques have to be converted to the real values. This is ensured by a set of equations. These equations need not only, the dimensionless forces and torques, but also the bearing dimensions (width, diameter and clearance) and oil properties (dynamic viscosity and density).

In future the hydrodynamic bearing model can be enriched by considering micro-lubrication (as presented by Maršálek in [7]). This would enable to consider the influence of the surface roughness.

### **3.4 Presumptions of the journal bearing model**

Since the model of the journal bearing is assembled in the way to enable solution in advance, several presumptions have to be considered. All the presumptions for the journal bearing model which were considered are as follows **Error! Reference source not found.:**

1. the journal and bearing shell shapes are ideal cylindrical parts,
2. the journal and the bearing shell are rigid bodies without any deformations, an oil gap between the journal and the shell is filled up with oil and the gap proportions are small in comparison with journal or bearing shell proportions,
3. only hydrodynamic friction can occur,
4. dynamic viscosity is constant for the whole gap volume and it is independent of local temperature and pressure,
5. lubricating oil is incompressible, and
6. oil flow is laminar.

### **3.5 Rotor model assembly**

There are essentially two possible approaches to assemble the turbocharger rotor model in MBS. The first one (shown in Fig. 2 a)) approach is to discretize the whole turbocharger rotor (compressor and turbine wheel, shaft, etc.) by the FE method. In this step all material characteristics have to be specified. In the second step the FE model is transferred into the format usable in MBS. This requires modal reduction of the model, namely Craig-Bampton reduction. This significantly reduces the number of DOF; and therefore, enables effective solution in time domain. In the last step the model is finished in MBS. Because the material, mass and geometry characteristics of the whole rotor are fixed from the FE model, it is more difficult to modify the design of the rotor. And therefore, this approach offers limited possibilities for parametric studies.

The second approach (shown in Fig. 2 b)) is based on considering only the shaft as flexible and both wheels (turbine and compressor wheel) and thrust collar as rigid. This approach relies on the assumption that the compressor and turbine wheel has greater stiffness; and therefore, has negligible deformation, if the

blade vibration is not considered. The blade vibration can be neglected if the overall rotor dynamics is analysed.

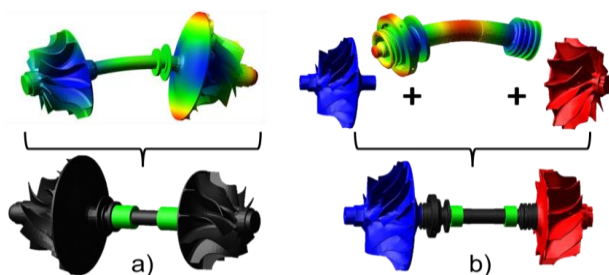


**Fig. 2.** Possible rotor modelling approaches: a) Fully flexible model, b) Flexible shaft with rigid wheels.

For assembling the model used for analysis presented in this paper the second approach was selected (shown in Fig. 2 b)). Since both the turbine and compressor wheel are considered rigid, as explained above, they do not allow analysis of blade vibration; but since their vibrations are mostly excited and affected by air/exhaust gases flow, the results would be misleading anyway.

Before the turbocharger model is fully completed, several other parts have to be added to the model. For example, if the floating ring bearing is considered, the floating rings have to be added to the model. The turbocharger housing model has to be considered as well – either flexible or rigid. The flexible housing offers more possibilities, e.g. vibration and noise analysis. But just for rotor dynamics analysis, the flexibility of the turbocharger housing can be neglected and the rigid housing will be sufficient. The influence of engine vibrations on turbocharger rotor dynamics can also be examined by introducing the excitation into the housing mounting points.

## 4. SIMULATION RESULTS

### 4.3 Simulation initial conditions

Before the results will be presented, it is necessary to present the initial conditions. Initial conditions introduced into turbocharger rotor dynamics simulation can be divided into several groups:

- 1) Rotor assembly conditions:
  - a) shaft is positioned in the middle of the floating ring ( $e_i=0$ ),

- b) floating rings are positioned in the middle of the housing bore ( $e_o=0$ ), and
- c) rotor speed is zero.

- 2) Loads acting on the rotor and bearing assembly (all of them are acting from the beginning of the simulation):

- a) gravity acting in the vertical direction (rotor assembly axis of rotation lies in the horizontal plane),
- b) oil pressure is 3.5 bar (the oil input pressure does not influence the rotor dynamics due to bearing model simplification, but it influences the bearing oil flow and oil warm up), and
- c) rotor assembly speed increases linearly. The rotor assembly is driven and the speed is controlled through the auxiliary body and torsional spring (the rotor speed can also be increased by the torque, but from the point of view of speed control, it is better to define the rotor speed).

- 3) Housing conditions:

- a) the housing is defined as a rigid body, and housing bore misalignment is neglected.

### 4.4 Influence of the compressor and turbine wheel mass and inertia on rotor dynamics

Since most modern turbochargers are created by redesigning the older ones, for turbocharger manufacturers it is important to have a knowledge of how an alteration of a single parameter will influence rotor dynamics of the turbocharger as a whole. Moreover, the design of a turbocharger, especially of turbine and compressor wheel, is often adjusted to perfectly fit a specific engine. And since the development of the turbocharger relies on measurement, it leads to many necessary experiments, which is an expensive and time consuming process.

The mass and inertia of the compressor and turbine wheel is often changed due to alteration of the material or wheel geometry. This is usually because of different operating conditions in the engine or demands on the turbocharger from the engine manufacturer.

For proper discussion of the influence of the compressor and turbine wheel mass and inertia change on rotor dynamics of a turbocharger, first the behaviour of the basic design has to be known. Furthermore, suitable parameters describing rotor dynamics have to be chosen. For this purpose the bearing eccentricity and waterfall diagram were selected.

The eccentricity of the bearing on the compressor side (the overall eccentricity of the floating ring bearing) is shown in Fig. 3. It can be clearly seen, that the eccentricity is fairly low up to the rotor speed of around  $40\,000\text{ min}^{-1}$ . Over this rotor speed, the overall eccentricity raises up to 0.6.

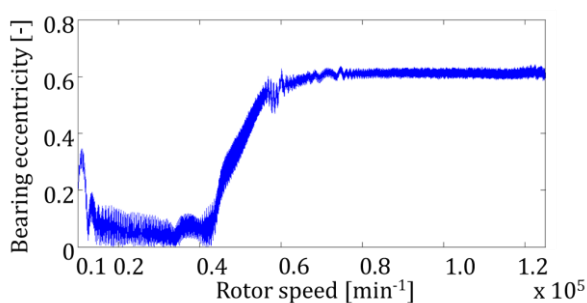


**Fig. 3.** Original design bearing eccentricity on the compressor side.

The cause of the increase of the eccentricity over the speed of  $40\,000\text{ min}^{-1}$  can be seen in a waterfall diagram in Fig 4. The cause of the higher eccentricity is the sub-synchronous vibration, which origins from the instability of the outer oil film. However, as our interest is the influence of the unbalance, it is necessary to look at the synchronous vibration since it is directly excited by it.

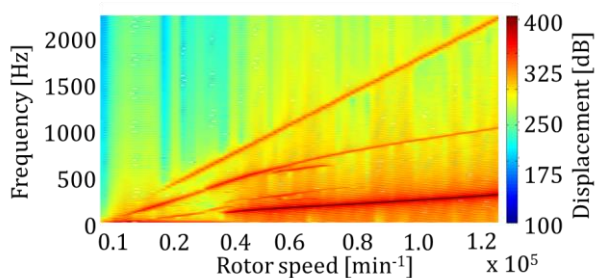


**Fig. 4.** Waterfall diagram of displacement on the compressor side of original design.

#### 4.5 Compressor wheel mass and inertia change

The coordinate system of the compressor wheel inertia is shown in Fig. 5. Through the simulations only the mass and inertia have been

changed. The location of the centre of gravity stayed the same. This represents the change of the material of the compressor wheel, i.e. its density.

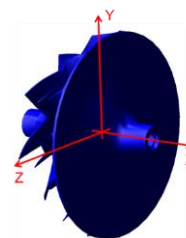


**Fig. 5.** Coordinate system of the compressor wheel inertia.

The mass and inertia of the compressor wheel have been changed according to the Table 1. At first, the original design was simulated and analysed and then the mass and inertia were increased by 10 % and 20 %, respectively. Then they were lowered by the same percentage.

**Table 1.** Compressor wheel mass and inertia considered in simulations.

	Mass [kg]	Inertia [kg·mm <sup>2</sup> ]		
		$I_{xx}$	$I_{yy}$	$I_{zz}$
Original design	0.20	110.00	80.00	80.00
10 % higher	0.22	121.00	88.00	88.00
20 % higher	0.26	145.20	105.60	105.60
10 % lower	0.24	130.68	95.04	95.04
20 % lower	0.19	104.54	76.03	76.03

The influence of the change of mass and inertia of the compressor wheel on the overall bearing eccentricity can be seen in Fig. 6 and Fig. 7. The Fig. 6 represents the influence on the overall bearing eccentricity of the bearing on the compressor side and the Fig. 7 on the turbine side.

The mean value of the overall bearing eccentricity of the bearing on the compressor side stays, through the speed range, almost identical except the speed range from  $40\,000\text{ min}^{-1}$  to  $60\,000\text{ min}^{-1}$  (Fig. 6). In this speed range the turbocharger rotor mounted with the compressor wheel with higher mass and inertia has higher eccentricity (up to 150 %), with respect to the initial design. As opposed to the turbocharger rotor mounted with the compressor wheel with lower mass and inertia has up to 80 % lower eccentricity than the initial design.

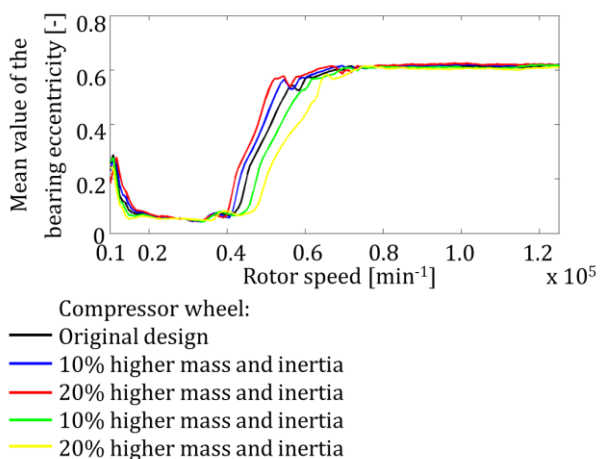


**Fig. 6.** Influence of the compressor wheel mass and inertia change on the mean value of overall bearing eccentricity on the compressor side

The overall bearing eccentricity of the bearing on the turbine side is much less influenced by the change of compressor design. The eccentricity values are nearly identical, except the speed range from 55 000 min<sup>-1</sup> to 75 000 min<sup>-1</sup> (Fig. 7). In this speed range the design with higher compressor mass and inertia has up to 35 % lower eccentricity relative to the initial design and the design with lower mass and inertia has up to the 60% higher eccentricity than the initial design.

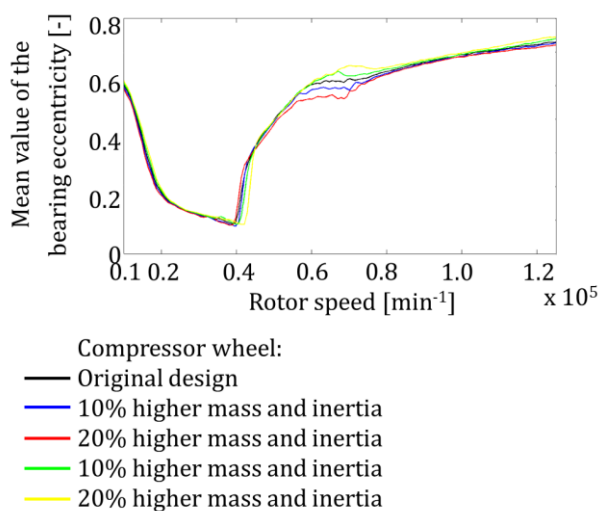


**Fig. 7.** Influence of the compressor wheel mass and inertia change on the mean value of overall bearing eccentricity on the turbine side

The difference in the bearing eccentricities can be understood through the frequency spectrum of the rotor vibration. This is represented by the waterfall diagrams in Fig. 8 - Fig. 11. Fig. 8 and Fig. 9 represent the waterfall diagram of the displacement on the compressor side and Fig. 10

and Fig. 11 represent the waterfall diagram of the displacement on the turbine side. Both of these displacements are measured on the wheel nose.

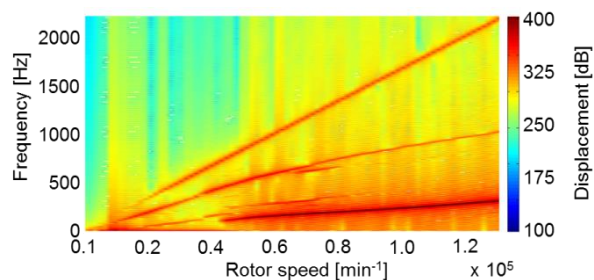


**Fig. 8.** Influence of the compressor wheel mass and inertia change on waterfall diagram of displacement on the compressor side (20 % lower compressor wheel mass and inertia).

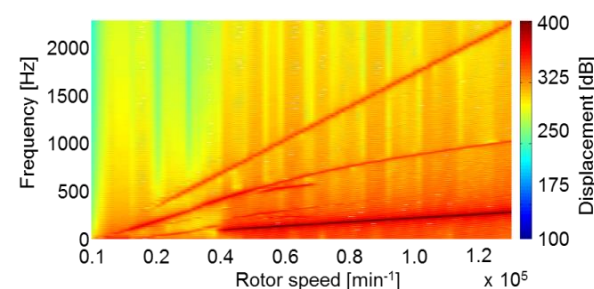


**Fig. 9.** Influence of the compressor wheel mass and inertia change on waterfall diagram of displacement on the compressor side (20 % higher compressor wheel mass and inertia).

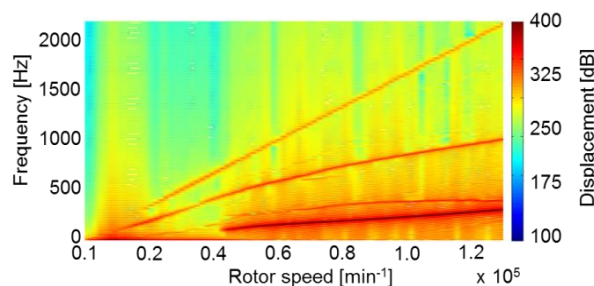


**Fig. 10.** Influence of the compressor wheel mass and inertia change on waterfall diagram of displacement on the turbine side (20 % lower compressor wheel mass and inertia).

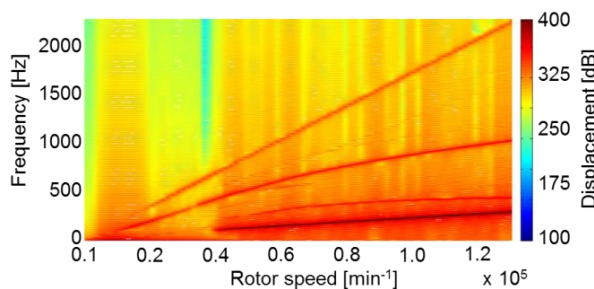


**Fig. 11.** Influence of the compressor wheel mass and inertia change on waterfall diagram of displacement on the turbine side (20 % higher compressor wheel mass and inertia).

### 4.6 Turbine wheel mass and inertia change

Similar to the characteristics of the compressor wheel, the turbine wheel characteristics were changed. The coordinate system of the turbine wheel inertia is shown in Fig. 12. All other conditions were similar to the previous analysis of the influence of the compressor wheel mass and inertia change. That means the same location of the centre of gravity.

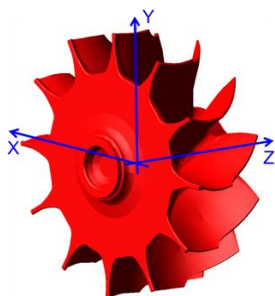


Fig. 12. Coordinate system of the turbine wheel inertia.

The mass and inertia of the turbine wheel have been changed according to the Table 2. At first, the original design was simulated and analysed and then the mass and inertia were increased by 10 %, and 20 % respectively, and then lowered by the same percentage.

Table 2. Turbine wheel mass and inertia considered in simulations.

	Mass [kg]	Inertia [kg·mm <sup>2</sup> ]		
		$I_{xx}$	$I_{yy}$	$I_{zz}$
Original design	0.50	160.00	160.00	190.00
10 % higher	0.55	176.00	176.00	209.00
20 % higher	0.66	211.20	211.20	250.80
10 % lower	0.59	190.08	190.08	225.72
20 % lower	0.48	152.06	152.06	180.58

Similar to the previous case, at first the overall bearing eccentricity of the bearing on the compressor and turbine side were analysed (Fig. 13 and Fig. 14). The eccentricities on the compressor side differ significantly only in the narrow speed range from 35 000 min<sup>-1</sup> to 60 000 min<sup>-1</sup> and for the design with 20 % higher mass and inertia above the speed of 110 000 min<sup>-1</sup>. The difference in the eccentricities is up to 90 % lower for the design with higher mass and inertia and up to 170 % higher for the design with higher mass and inertia.

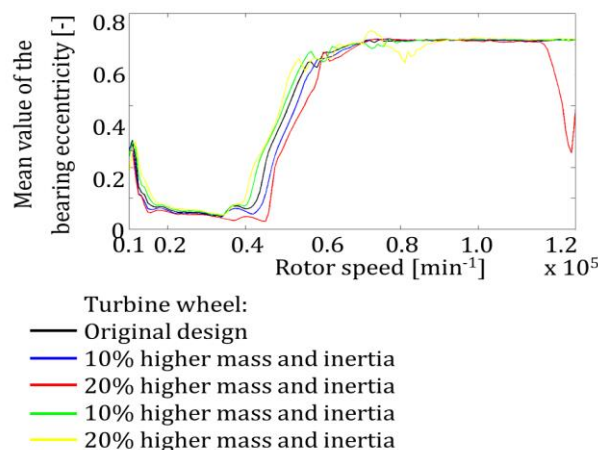


Fig. 13. Influence of the turbine wheel mass and inertia change on the mean value of overall bearing eccentricity on the compressor side.

The behaviour of the bearing eccentricity on the turbine side is significantly influenced by the change of turbine mass and inertia, as shown in Fig. 14. Eccentricities of the modified designs are different throughout the whole speed range. The turbine with higher mass and inertia leads to higher eccentricity and, as expected, the turbine with lower mass and inertia leads to lower eccentricity.

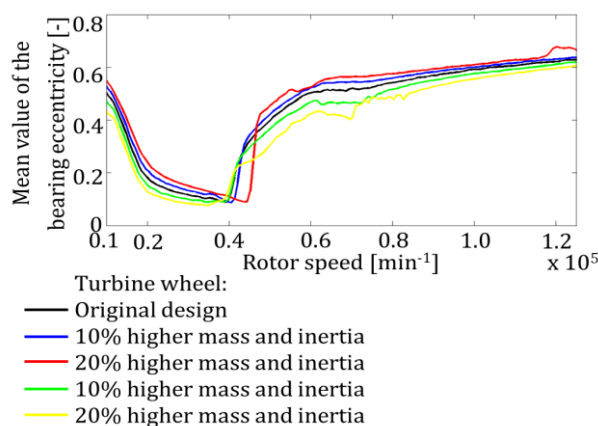


Fig. 14. Influence of the turbine wheel mass and inertia change on the mean value of overall bearing eccentricity on the turbine side

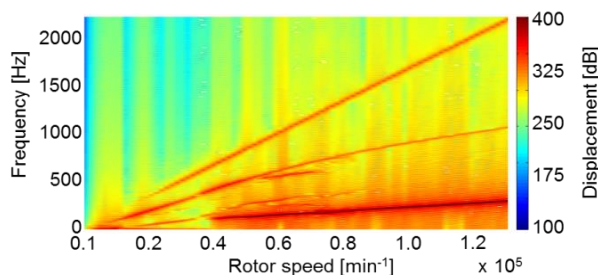
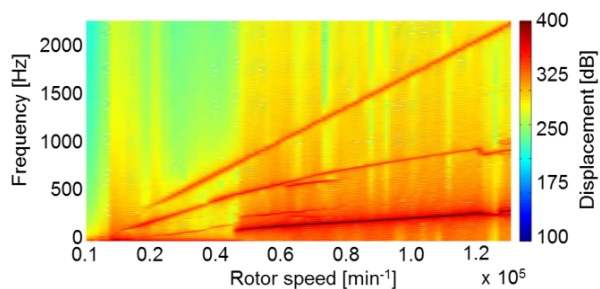
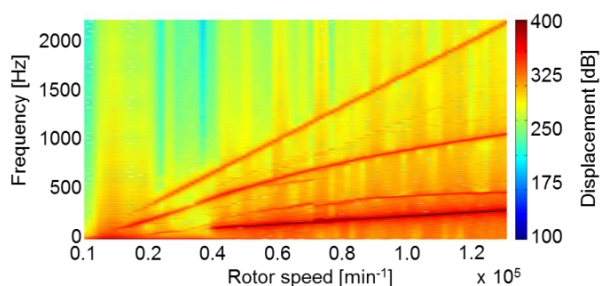


Fig. 15. Influence of the turbine wheel mass and inertia change on waterfall diagram of displacement on the compressor side (20 % lower turbine wheel mass and inertia).



**Fig. 16.** Influence of the turbine wheel mass and inertia change on waterfall diagram of displacement on the compressor side (20 % higher turbine wheel mass and inertia).



**Fig. 17.** Influence of the turbine wheel mass and inertia change on waterfall diagram of displacement on the turbine side (20 % lower turbine wheel mass and inertia).

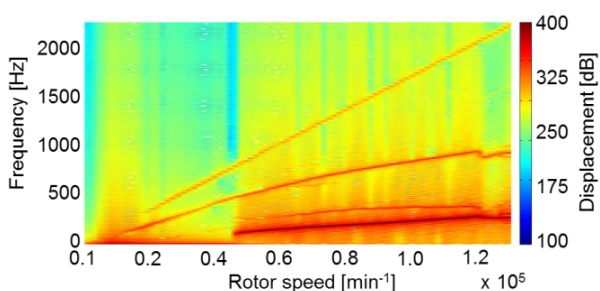


**Fig. 18.** Influence of the turbine wheel mass and inertia change on waterfall diagram of displacement on the turbine side (20 % higher turbine wheel mass and inertia).

The waterfall diagrams of displacements on the compressor and turbine wheel noses are shown in Fig. 15 - Fig. 18.

## 5. CONCLUSION

Since mass and inertia of the compressor and turbine wheel are often changed to meet the demands placed on the turbocharger, it is vital to know the influence of these changes on rotor dynamics. This influence can be seen in figures above. It is clear, that up to the 20 % difference in wheel mass and inertia the influence is not so significant. However, it has to be pointed out

that during the wheel design change the location of the centre of gravity is usually shifted. And in this paper the centre of gravity has been considered to be at the same location.

But even though the influence on the rotor dynamics is not significant, each case should be analysed separately. There are generally two ways to check the influence on rotor dynamics – measurement and simulation. Since the measurement is time consuming and expensive it is advantageous to use simulation tools to perform analysis of several designs and then, just for final verification, use measurement. This approach can significantly reduce development time and costs of a new turbocharger.

## Acknowledgement

The research leading to these results has received funding from the Ministry of Education, Youth and Sports under the National Sustainability Programme I (Project LO1202).

## REFERENCES

- [1] B. SCHWEIZER, N.F. RIEGER, H.F. BLACK, N.F. RIEGER and Ch.B. THOMAS, 'Dynamics and stability of turbocharger rotors', *Archive of Applied Mechanics*, vol. 80, no. 9, pp. 436-471, 2010.
- [2] B. SCHWEIZER, 'Dynamics and stability of turbocharger rotors', *Archive of Applied Mechanics*, vol. 80, no. 9, pp. 1017-1043, 2010.
- [3] L. TIAN, W.J. WANG and Z.J. PENG, 'Dynamic behaviors of a full floating ring bearing supported turbocharger rotor with engine excitation', *Journal of Sound and Vibration*, vol. 330, no. 20, pp. 4851-4874, 2011.
- [4] L. TIAN, W.J. WANG and Z.J. PENG, 'Nonlinear effects of unbalance in the rotor-floating ring bearing system of turbochargers', *Mechanical Systems and Signal Processing*, vol. 34, no. 1-2, pp. 298-320, 2013.
- [5] P. NOVOTNÝ, *Virtual Engine: A Tool for Powertrain Development*. Brno, Inaugural Dissertation. Brno University of Technology, 2009.
- [6] O. Maršálek, *Advanced Methods for the Solution of Journal Bearing Dynamics*. Brno, Dissertation. Brno University of Technology, 2015.
- [7] O. Maršálek, P. Novotný and P. Raffai, 'Micro-lubrication of Directionally Oriented Contact

Surfaces', *Tribology in Industry*, vol. 36, no. 4, pp. 451-464, 2014.

[8] B. Nedić, S. Perić and M. Vuruna, 'Monitoring Physical and Chemical Characteristics Oil for Lubrication', *Tribology in Industry*, vol. 31, no. 3&4, pp. 59-66, 2009.

[9] K.A. Nuzhdin, V.M. Musalimov and I.I. Kalapyshina, 'Modelling of Nonlinear Dynamic of

Mechanic Systems with the Force Tribological Interaction', *Tribology in Industry*, vol. 37, no. 3, pp. 366-373, 2015.

[10] S. Baskar and G. Sriram, 'Tribological Behavior of Journal Bearing Material under Different Lubricants', *Tribology in Industry*, vol. 36, no. 2, pp. 127-133, 2014.